RSC Advances

PAPER

View Article Online
View Journal | View Issue

Cite this: *RSC Adv.*, 2019, **9**, 24377

Tunable preparation of highly dispersed Ni_xMn-LDO catalysts derived from Ni_xMn-LDHs precursors and application in low-temperature NH_3-SCR reactions†

Benhui Hou,[a] Yali Du,[b] Xuezhen Liu,[a] Chao Ci,[a] Xu Wu *[a] and Xianmei Xie*[a]

Received 18th June 2019
Accepted 25th July 2019

DOI: 10.1039/c9ra04578c

rsc.li/rsc-advances

A series of Ni_xMn bimixed metal oxides (Ni_xMn-LDO) were prepared *via* calcining Ni_xMn layered double hydroxides (Ni_xMn-LDHs) precursors at 400 °C and applied as catalysts in the selective catalytic reduction (SCR) of NO_x with NH_3. The $DeNO_x$ performance of catalysts was optimized by adjusting the Ni/Mn molar ratios of Ni_xMn-LDO precursors, in which Ni_5Mn-LDO exhibited above 90% NO_x conversion and N_2 selectivity at a temperature zone of 180–360 °C. Besides, Ni_5Mn-LDO possessed considerable SO_2 & H_2O resistance and outstanding stability. Multiple characterization techniques were used to analyze the physicochemical properties of the catalysts. The analysis results indicated that all catalysts had the same active species Ni_6MnO_8, while their particle sizes showed significant differences. Notably, the uniform distribution of active species particles in the Ni_5Mn-LDO catalyst provided the rich surface acidity and suitable redox ability which were the primary causes for its desirable $DeNO_x$ property.

1. Introduction

During the past decades, nitrogen oxide (NO_x) emissions have increased dramatically, which triggered a battery of environmental problems including photochemical smog, acid rain and greenhouse effects, further endangering human health.[1,2] With the increasingly severe strictness of environmental regulations, it is necessary to find a valid method to eliminate NO_x. Among numerous removal techniques, selective catalytic reduction of NO_x with NH_3 (NH_3-SCR) has been considered as the most effective measure for denitrification ($DeNO_x$).[3,4] Currently, commercial catalysts V_2O_5–WO_3/TiO_2 have been widely used in the field of industrial stationary sources, which displayed good catalytic performance at the high temperature region of 300–400 °C.[5] However, V-based catalysts still possess defects, such as the narrow operation temperature window, low N_2 selectivity at higher temperatures and inherent toxicity, which restricted its further application.[6] Thus, it is worthwhile to develop non-toxic $DeNO_x$ catalysts with good low temperature activity.

Based on the features of environmentally friendly and variable valence of Mn element, MnO_x has been deemed as the potential catalyst for NH_3-SCR reaction in the low temperature zone.[7–9] Whereas there were some inevitably problems caused by its stronger oxidation capacity which easily led to the over-oxidation of NH_3 at higher temperature and further reduced SCR activity as well as N_2 selectivity.[10,11] Recently, it has been reported that the strong oxidation capacity of MnO_x catalyst could be adapted by introducing transition metals.[12–15] Among all the attempts, Ni was considered to be a functional component with excellent synergistic catalysis. For instance, Wan *et al.*[16] and Chen *et al.*[17] prepared Ni–Mn bi-metal oxides and Ni–Mn spinel oxides catalysts, respectively, the catalytic performance results showed that both catalysts exhibited higher SCR activity and N_2 selectivity than single MnO_x catalyst. Although some progress has been made, it was unavoidable that the active specie particles of Ni–Mn catalysts prepared by traditional methods were prone to agglomerate, resulting in the decline of catalytic performance.[18]

As investigated in the previous studies, the dispersion of active specie particles over catalyst could be effectively improved *via* regulating the morphology and structure.[19–21] Lately, the layered double oxides (LDO) catalysts obtained *via* calcining layered double hydroxides (LDHs) precursor attracted proverbial attention due to the excellent physical and chemical properties.[22–24] Moreover, our group have also found that the catalysts prepared by employing LDHs as precursor could achieve better SCR activity than other methods, it might be related with the lattice limiting effect and surface hydrazine structure existed in bulk laminate of LDHs, which were helpful to improve the dispersion and stability of the active specie particles.[25]

[a]College of Chemistry and Chemical Engineering, Taiyuan University of Technology, Taiyuan 030024, PR China. E-mail: wuxu@tyut.edu.cn; xxmsxty@sina.com; Fax: +86-351-6018528; +86-351-6018564; Tel: +86-351-6018528; +86-351-6018564

[b]College of Chemistry and Chemical Engineering, Jinzhong University, Jinzhong 030619, PR China

† Electronic supplementary information (ESI) available. See DOI: 10.1039/c9ra04578c

In this work, on account of the synergistic effect of Ni and Mn as well as satisfactory function of LDHs, Ni_xMn-LDHs with different Ni/Mn molar ratios were successfully fabricated with aid of coprecipitation methods. Ni_xMn-LDO obtained by calcining Ni_xMn-LDHs at a proper temperature were hired as $DeNO_x$ catalysts in NH_3-SCR reaction. In order to optimize physical and chemical properties of Ni_xMn-LDO catalysts, the relative proportions of Ni and Mn of the Ni_xMn-LDHs precursors were explored in detail. A series of characterization techniques were used to reveal the intrinsic reason for the differences in catalytic activities among catalysts. This research might expand a new horizon to develop new catalysts with outstanding efficiency.

2. Experimental section

2.1 Preparation of catalysts

The Ni_xMn-LDHs ("x" represent Ni/Mn molar ratio = 3, 4, 5, 6 and total molar amount Ni + Mn = 0.06 mol) were prepared by co-precipitation method.[26] To be specific, for the synthesis of Ni_3Mn-LDHs, 0.045 mol (13.09 g) of $Ni(NO_3)_2{\cdot}6H_2O$ (98.0%) and 0.015 mol (5.37 g) of $Mn(NO_3)_2$ (50%) were dissolved in 100 mL deionized water to prepare metal precursor solution. The mixed alkali solution were obtained by dissolving 0.04 mol (1.6 g) of NaOH and 2.8 g of $NH_3{\cdot}H_2O$ (25–28%) in 100 mL deionized water. Then, the metal precursor solution and alkali solution were simultaneously added dropwise with magnetic stirring into flask at room temperature. The suspension was crystallized at 80 °C for 24 h, and then the resulting subsidence by filtration, washing and drying at 80 °C for 12 h to obtain the Ni_3Mn-LDH precursor. The Ni_3Mn-LDO catalyst was obtained by calcining Ni_3Mn-LDHs precursor in air at 400 °C for 5 h at a heating rate of 2 °C min^{-1}. Similarly, other samples such as Ni_4Mn-LDO, Ni_5Mn-LDO and Ni_6Mn-LDO were obtained with the same method.

2.2 Characterization of catalysts

X-ray diffraction (XRD) information of catalysts was measured on a Rigaku DX-2700 instrument using Cu/Kα radiation source. The 2θ range of meterage from 5 to 85° and a scanning rate was 8° min^{-1}. The Ni and Mn contents were determined by inductively coupled plasma-atomic (ICP) on Optima 7000 DV instrument. Fourier transform infrared spectrometer (FT-IR) experiment were tested from 400 to 3600 cm^{-1} on a TENSOR II FT-IR (Bruker). Thermogravimetry (TG) analyzer (Setaram Evolution) equipped with quadrupole mass spectrometry (QMS) real-time monitored the thermal decomposition of LDHs sample with the temperature rising from 50 °C to 800 °C. The surface area and pore information of catalysts were obtained by using Brunauer–Emmett–Teller (BET) and Barrett–Joyner–Halenda (BJH) methods on Micromeritics ASAP-2460 apparatus. The test conditions are mainly that the catalyst samples were degassed at 250 °C for 4 h. Ammonia-temperature programmed desorption (NH_3-TPD) was performed on FINESORB-3010C chemisorptions analyzer with thermal conductivity detector (TCD). About 100 mg catalysts (40–60 mesh) was pretreated at 300 °C for 1 h under 25 mL min^{-1} He atmosphere; subsequently, the sample adsorbed NH_3 to achieve saturation at 50 °C for 1 h and He was purged at the same temperature to remove weakly adsorbed NH_3 on the surface; finally, the desorption curve was recorded *via* increasing temperature (from 50 °C to 560 °C) with heating rate of 10 °C min^{-1} under 25 mL min^{-1} He atmosphere. Hydrogen-temperature programmed reduction (H_2-TPR) was tested in the same way. About 80 mg catalysts was pretreated at 300 °C for 1 h under 30 mL min^{-1} Ar atmosphere; after cooling down to 50 °C, the catalyst samples accomplished the reduction process from 80 °C to 800 °C in a flow of 30 mL min^{-1} 10% H_2/Ar. In order to explore the surface morphology and structure of the sample, scanning electron microscope (SEM) and high resolution-transmission electron microscopy (HR-TEM) were conducted on a Hitachi SU8010 apparatus and JEM-2100F (JEOL) with an accelerating voltage of 200 kV, respectively. The EDS equipped with SEM was also used to characterize the surface composition of catalyst.

2.3 Activity measurements of catalysts

The SCR activity measurements of catalysts were carried out on a fixed-bed quartz reactor with the internal diameter of 6 mm. About 350 mg catalyst samples (40–60 mesh) were placed in the reactor. The reaction gas composition was as follows: 600 ppm NO, 600 ppm NH_3, 5 vol% O_2, 10 vol% H_2O (when used), 100 ppm SO_2 (when used) and N_2 as the balance gas. The total flow rate of gas was 187 mL min^{-1} and GHSV = 45 000 h^{-1}. The activity performance were tested at range from 90 to 390 °C and the data were collected for every 30 °C, meanwhile, the output gases were monitored by multigas 2000 FTIR. The NO_x conversion and N_2 selectivity were calculated as follows:

$$NO_x\ \text{conversion} = 100\% \times ([NO_x]_{in} - [NO_x]_{out})/[NO_x]_{in}$$

$$N_2\ \text{selectivity} = 100\% \times ([NO_x]_{in} + [NH_3]_{in} - [NO_x]_{out} - [NH_3]_{out} - 2[N_2O]_{out})/([NO]_{in} + [NH_3]_{in} - [NO_x]_{out} - [NH_3]_{out})$$

where "in" represents the gas concentration at the inlet, "out" represents the gas concentration at the output.

3. Results and discussion, experimental

3.1 Characterization of Ni_xMn-LDHs precursors

3.1.1 XRD analysis. XRD patterns of the Ni_xMn-LDHs precursors with different Ni/Mn molar ratios were displayed in Fig. 1. As the results presented, all samples showed the typical diffraction peaks at about 11.0°, 22.1°, 34.3°, 38.7°, 45.0°, 60.0° and 61.1°, which can be indexed to (003), (006), (012), (015), (018), (110) and (113) planes of Ni_xMn-LDHs,[27–29] and no other miscellaneous peaks were observed. That is to say, Ni_xMn-LDHs with pure phase were synthesized successfully. It can be seen that the (003) diffraction peaks of four samples appear at 11°, further the basal spacings of Ni_xMn-LDHs were calculated as 8.04 Å by Bragg's equation of $n\lambda = 2d \sin\theta$, which indicated that CO_3^{2-} existed in the interlayers of LDHs.[26,30] In addition,

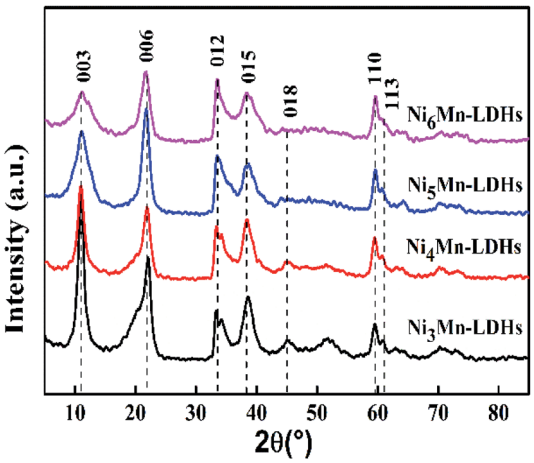

Fig. 1 XRD patterns of Ni_xMn-LDHs precursors (x = 3, 4, 5, 6).

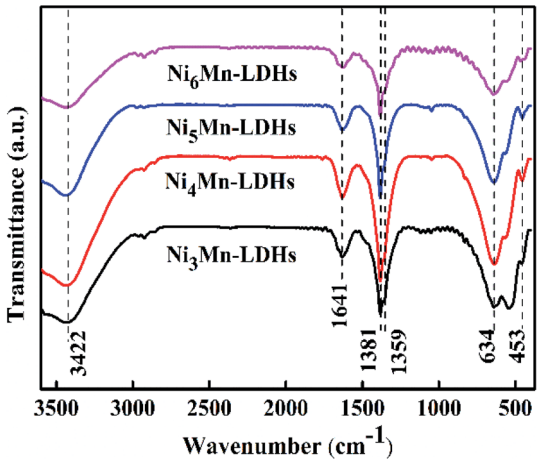

Fig. 2 FT-IR spectra of Ni_xMn-LDHs precursors (x = 3, 4, 5, 6).

with the increase of Ni/Mn molar ratios for Ni_xMn-LDHs, it can be observed that the intensity of the (003) diffraction peaks showed a tendency to reduce, and the peaks width became wider. This implied that Ni_5Mn-LDHs and Ni_6Mn-LDHs possessed smaller LDHs crystal sizes compared with Ni_3Mn-LDHs and Ni_4Mn-LDHs (Table 1), which may change the appearance of the LDHs precursors and thus affect the dispersibility of the calcined product. Furthermore, tested Ni/Mn molar ratios were determined by ICP analysis (Table 1), and the result was consistent with feeding ratios. The composition and morphology information of the Ni_xMn-LDHs were further investigated by FT-IR and SEM.

3.1.2 FT-IR analysis. Fig. 2 showed the FT-IR spectra for Ni_xMn-LDHs (x = 3, 4, 5, 6). It could be found that a series of infrared adsorption bands were displayed within the wavenumber range of 400–3600 cm^{-1}. Broad adsorption band at 3422 cm^{-1} could be assigned to stretching vibration of –OH groups in the Ni_xMn-LDHs layers and interlayer water molecules.[31] The adsorption band at 1641 cm^{-1} might be due to the angular deformation of water.[32] The vibration of CO_3^{2-} and NO_3^- existed in interlayers could be observed at 1381 and 1359 cm^{-1}, respectively.[26] Additionally, the adsorption bands around 634 and 453 cm^{-1} could be attributed to the cation-oxygen vibrations, such as O–M–O, M–O–M or M–OH.[33] These results further indicated that the prepared Ni_xMn-LDHs samples were CO_3^{2-} and NO_3^- intercalated.

Table 1 Chemical compositions and XRD parameters of Ni_xMn-LDHs (x = 3, 4, 5, 6) precursors

	Weight content[a]				
Samples	Ni	Mn	Ni : Mn	$FWHM_{003}$	D_{003}[b] (nm)
Ni_3Mn-LDHs	44.37	15.32	2.89	0.0164	8.39
Ni_4Mn-LDHs	47.66	12.41	3.84	0.0170	8.09
Ni_5Mn-LDHs	49.01	9.55	5.13	0.0216	6.40
Ni_6Mn-LDHs	51.22	8.71	5.88	0.0222	6.21

[a] Weight content of Ni and Mn was determined by ICP analysis. [b] D_{003} of samples was calculated by Scherrer equation.

3.1.3 SEM analysis. The SEM characterization was adopted to probe the microscopic morphology of the precursors, the corresponding results were shown in Fig. 3. As can be seen, the four samples exhibited typical nanosheet structure, which might further witnessed the successful synthesis of LDHs precursors.[34,35] Moreover, it could also be observed that surface morphology of four samples has changed obviously with the increase of Ni/Mn molar ratios. For Ni_3Mn-LDHs and Ni_4Mn-LDHs, the LDHs sheets presented a larger size and seriously stacked, which will greatly affect the exposure of the effective components on the surface of the sample. In contrast, the sheets size of Ni_5Mn-LDHs and Ni_6Mn-LDHs was significantly reduced and the degree of accumulation was greatly improved. In fact, thus morphology difference of precursor often influence the properties of the calcined product.

3.1.4 TG-MS analysis. The thermal decomposition of the Ni_xMn-LDHs precursors was clearly explored by TG-MS analysis. As shown in Fig. 4, take Ni_5Mn-LDHs as an example. Three distinct weight loss peaks appeared on the curves of TG and DTG (Fig. 4(a)). The first weight loss stage around 80–130 °C was caused by the removal of physically adsorbed water, interlayer

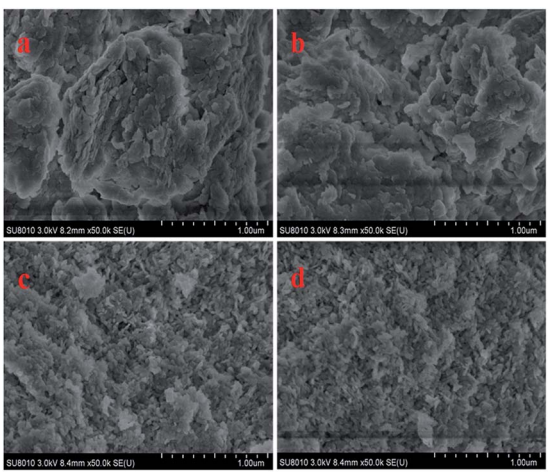

Fig. 3 SEM images of (a) Ni_3Mn-LDHs; (b) Ni_4Mn-LDHs; (c) Ni_5Mn-LDHs and (d) Ni_6Mn-LDHs precursors.

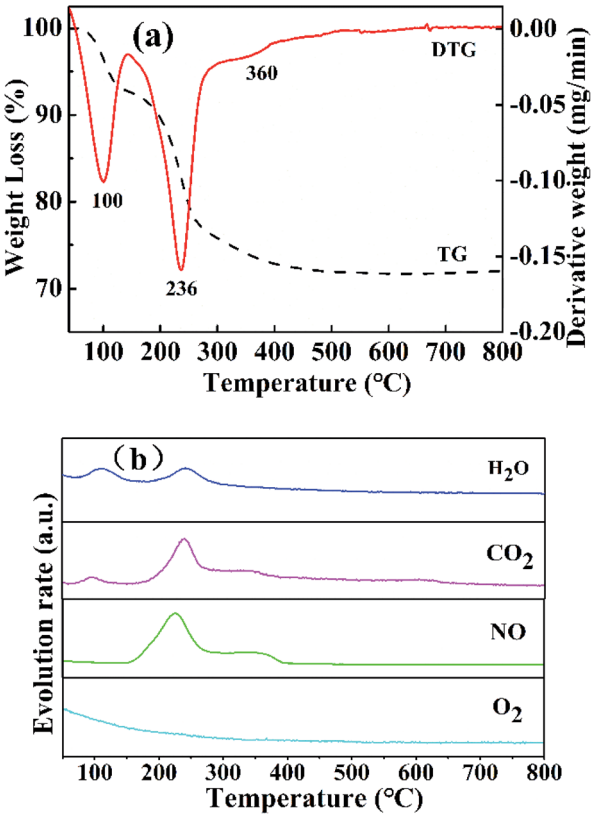

Fig. 4 Curves of TG and DTG (a) and MS (b) for Ni_5Mn-LDHs samples.

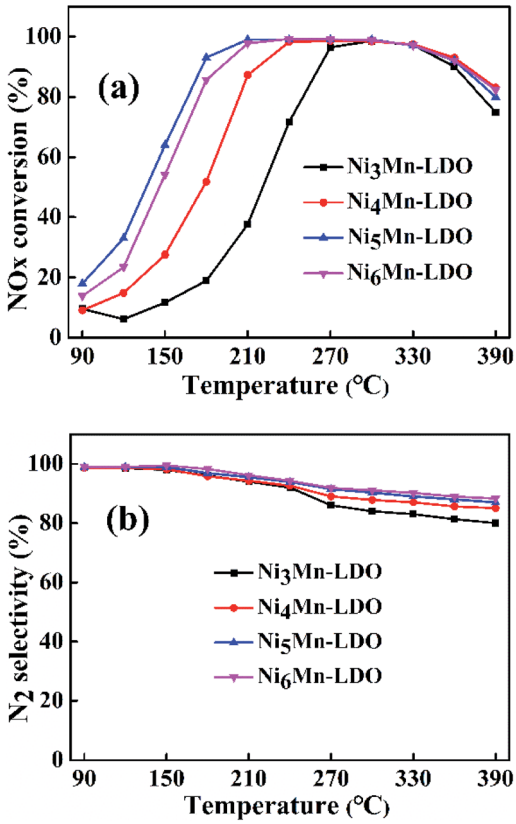

Fig. 5 (a) NO_x conversion and (b) N_2 selectivity of Ni_xMn-LDO ($x = 3$, 4, 5, 6) catalysts. Reaction conditions: [NO] = [NH_3] = 600 ppm, [O_2] = 5 vol%, N_2 as balance gas, GHSV = 45 000 h^{-1}.

water and CO_2 molecules, where the release signal of the corresponding gases (H_2O and CO_2) was detected by MS (Fig. 4(b)).[36] The major weight loss process occurred at second stage, which took place at the temperature range of 150–300 °C, mainly arising from the dehydration of –OH group on the LDHs laminate as well as the loss of volatile gases CO_2 and NO from the interlayer CO_3^{2-} and NO_3^- ions.[37] The last weight loss stage displayed a slight exothermic peak at about 360 °C, a small amount of CO_2 and NO release can be still observed from MS (Fig. 4(b)), which can be assigned to decomposition of interlayer anions CO_3^{2-} and NO_3^- at higher temperature.[32] As the temperature further increased (>400 °C), no weight loss peak was found, indicating that the Ni_5Mn-LDHs precursor achieved complete decomposition. Based on the TG-MS analysis, it can be concluded that calcining LDHs precursors at 400 °C can form stable mixed metal oxides.

3.2 Characterization of Ni_xMn-LDO ($x = 3$, 4, 5, 6) catalysts

3.2.1 SCR performance of Ni_xMn-LDO ($x = 3$, 4, 5, 6) catalysts. SCR activity and N_2 selectivity of Ni_xMn-LDO catalysts with different metal molar ratios (Ni/Mn = 3, 4, 5, 6) were tested under a GHSV of 45 000 h^{-1}. As illustrated in Fig. 5(a), the NO_x conversion of all catalysts has experienced three stages at the test temperature range of 90–390 °C. At the first stage, the NO_x conversion of Ni_xMn-LDO catalysts increased sharply with increasing temperature and gradually reached the maximum of 98%. Followed by the second stage, the NO_x conversion substantially remained at 98% without obvious changes. On the third stage, the NO_x conversion presented a declining trend. Notably, it can be observed that the NO_x conversion of Ni_xMn-LDO catalysts were significantly influenced by Ni/Mn molar ratios on the first stage. When the Ni/Mn molar ratios rose from 3 to 5, the NO_x conversion over Ni_xMn-LDO catalysts displayed an upward trend, Ni_5Mn-LDO catalyst afforded the best catalytic activity. However, when the Ni/Mn molar ratios was further increased, Ni_6Mn-LDO exhibited lower activity than the Ni_5Mn-LDO catalyst, which might be related to the further reduction of the Mn content. Thus, the SCR activity of different catalysts presented as the following order: Ni_5Mn-LDO > Ni_6Mn-LDO > Ni_4Mn-LDO > Ni_3Mn-LDO. In order to further understand the catalytic performance of the Ni_xMn-LDO catalysts, the SCR activity comparison of present catalyst and the other Ni–Mn catalysts in literatures was involved in Table S1.† As the result presented that Ni_xMn-LDO catalyst exhibited different activity temperature windows, which may be related to the structural composition of the LDHs precursors.

The N_2 selectivity of Ni_xMn-LDO catalysts was also considered. As shown in Fig. 5(b), all catalysts exhibited similar N_2 selectivity about 85% or higher over the entire temperature range. Whereas, with the temperature raising and exceeding 180 °C, the N_2 selectivity of each catalyst decreased to varying degrees, in which Ni_5Mn-LDO and Ni_6Mn-LDO catalysts displayed better N_2 selectivity than the other two. These results

indicated that SCR performance of Ni_xMn-LDO could be affected by the Ni/Mn molar ratios.

3.2.2 XRD analysis. Fig. 6 gave XRD patterns of Ni_xMn-LDO catalysts. As can be seen from the diagram, all catalysts exhibited a similar XRD characteristic diffraction peaks. The peaks located at 18.7°, 37.3°, 43.4°, 63.1° can be attributed to Ni_6MnO_8 phase (JCPDS 49-1295).[38] The appearance of Ni_6MnO_8 crystal phase can be related to the formation of Mn–Ni–O solid solution, which is mainly because that part of Mn^{3+} and Mn^{4+} can insert the lattice of NiO where the radius of Ni^{2+} (0.069 nm) is greater than Mn^{3+} (0.066 nm) and Mn^{4+} (0.056 nm).[39] It was reported that the phase of Ni_6MnO_8 was conducive to the improvement of SCR activity.[20] The peaks at 2θ of 37.3°, 43.4°, 63.1°, 75.5°, 79.7°can be assigned to NiO phase (JCPDS 75-0197),[38,39] it was partially overlapped with those of Ni_6MnO_8 and can be further analyzed by TEM. Meanwhile, the absence of the diffraction peaks for pure MnO_x may be due to that a part of Mn participated in the formation of Ni_6MnO_8 and remained Mn existed in an amorphous state. In addition, with the increase of Ni/Mn molar ratios for Ni_xMn-LDO, diffraction peaks of samples were broadened and its intensity descended, indicating the gradual decreasing of crystal size. Generally speaking, small crystal can expose more crystal defects, which is more beneficial to improving catalytic activity.[39] This well explained the difference in catalytic activity for catalysts to some extent.

3.2.3 SEM, TEM and HRTEM analysis. The degree of exposure of catalyst surface active species is an important factor affecting catalytic activity.[40] Therefore, the surface information of Ni_xMn-LDO catalyst was investigated by SEM and TEM. Above all, the SEM images of four catalysts were shown in Fig. S1–S4.† After 400 °C calcination, all samples exhibited a spherical morphology and the sheet structure disappeared completely, which indicated that the LDHs laminate collapsed and a stable composite metal oxide formed. To further explore the surface element composition of the catalyst, the EDS mapping of Ni_xMn-LDO catalysts was also conducted, as shown in Fig. S1–S4.† It can be seen that the O, Ni and Mn element was well dispersed on the surface of the catalyst. In addition, based on the relative content of Ni and Mn elements of each catalyst, surface Ni/Mn molar ratios of four samples was calculated. For Ni_5Mn-LDO catalyst, it was noticed that its Ni/Mn molar ratios (4.68) was much lower than tested value (5.13) determined by ICP analysis. This result suggested that more Mn elements can be fully exposed on the catalyst surface and further enhancing SCR activity, which may be related to the uniform distribution of metal oxide particles in the catalyst.

Then the TEM images of Ni_xMn-LDO catalysts were shown in Fig. 7(a–d), it can be clearly observed that the active nanoparticles are anchoring on the catalyst surface, but there are some difference in dispersion with Ni/Mn molar ratios change of catalysts. As for Ni_3Mn-LDO and Ni_4Mn-LDO catalysts, a portion of active species particles have undergone significant agglomeration, with the corresponding average particle size being 17.67 nm and 15.68 nm, respectively. In contrast, the aggregation degree of active nanoparticles for Ni_5Mn-LDO and Ni_6Mn-LDO catalysts was improved significantly with the average particle size being 13.23 nm and 12.51 nm, respectively. Combined with the SEM analysis of the Ni_xMn-LDHs samples, it can be concluded that the morphological difference of the precursors can seriously affect the exposure opportunities of catalyst surface active species. This result revealed that higher catalytic activity was achieved to Ni_5Mn-LDO and Ni_6Mn-LDO catalysts. In order to further investigate the phase composition of the catalyst, HRTEM analysis of Ni_xMn-LDO was carried out in this part. As compiled in Fig. 7(e–h), all catalysts exhibited two different types of lattice fringes, the lattice spacings of 0.239 nm can be assigned to the (222) plane of NiO, and the lattice spacings of 0.211 nm correspond to Ni_6MnO_8 (400) plane,[39] which is in good accordance with the XRD analysis results.

3.2.4 N_2 adsorption–desorption analysis. The N_2 adsorption–desorption characterization was used to test the surface area and pore structure distribution of the Ni_xMn-LDO catalysts. Related results were shown in Fig. 8(a and b) and Table 2. As illustrated in Fig. 8(a), four catalysts exhibit the same type of desorption curves belonging to type IV isotherms with type H2 hysteresis loops, which fully indicated the existence of mesoporous structure.[34,41,42] The corresponding pore diameter distribution was considered in Fig. 8(b). It can be observed that the sample of Ni_3Mn-LDO has a wide pore size distribution with 10–40 nm. Comparatively, the pore size distribution range of Ni_xMn-LDO (x = 4, 5, 6) was greatly reduced and more concentrated around 5–20 nm, which implies that the latter had a more uniform pore size structure.[43] Moreover, the surface area was obtained in Table 2 by calculating with BET method. Obviously, the surface area value of samples was sensitive to the proportion of Ni/Mn and displayed an upward trend from 41 to 83 $m^2\ g^{-1}$ with enhancement of Ni/Mn molar ratios. Combined with TEM analysis, thus may be related to the uniform distribution of the active species particles. Generally, a large specific surface area can provide maximum active and adsorption sites, which might be favorable to the improvement of catalytic activity.[44] The Ni_5Mn-LDO catalyst presented a large specific surface area (70 $m^2\ g^{-1}$), suitable average pore diameter (9.35

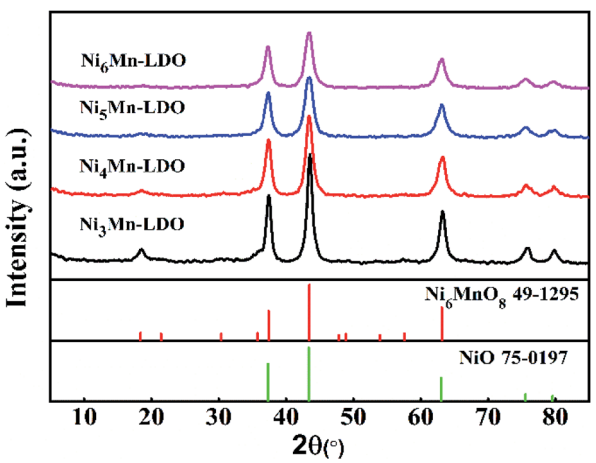

Fig. 6 XRD patterns of Ni_xMn-LDO (x = 3, 4, 5, 6) catalysts.

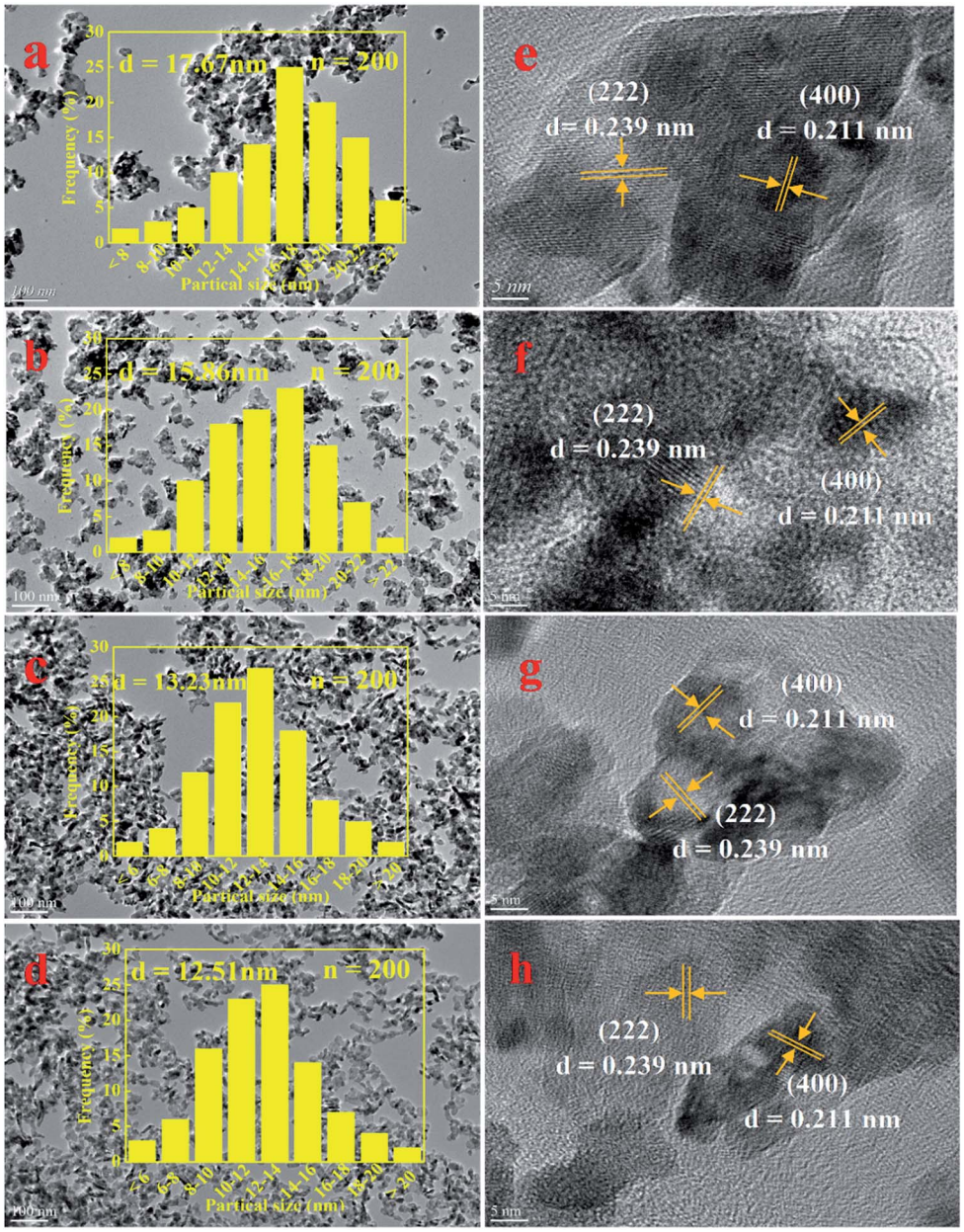

Fig. 7 (a–d) TEM and (e–h) HRTEM images of Ni_xMn-LDO catalysts: (a, e) Ni_3Mn-LDO; (b, f) Ni_4Mn-LDO; (c, g) Ni_5Mn-LDO; (d, h) Ni_6Mn-LDO.

nm) and pore volume (0.17 $cm^3\ g^{-1}$), resulting in the desirable SCR activity.[43,45]

3.2.5 NH_3-TPD analysis. In NH_3-SCR reaction, the adsorption and activation of NH_3 by catalyst is an important factor affecting the $DeNO_x$ action.[41,46] Therefore, surface acidity of all catalysts was measured by NH_3-TPD experiment (Fig. 9). As can be seen, the four catalysts exhibited two similar NH_3 desorption peaks in the test temperature range with 50–560 °C. The peak at lower temperature with 50–300 °C was considered to be the desorption of weak acid sites on the catalyst surface, which can be attributed to NH_4^+ ions bound to the Brønsted acid sites.[41,47,48] The desorption peak at high temperature with 350–550 °C was usually caused by coordinated NH_3 molecular originating from the Lewis acid sites with stronger acidity, which might be because that the complex formed by the NH_3 lone pair electron coordination possess stronger thermal stability than the NH_4^+ ions.[49–52] Since the desorption peak positions of the four catalysts were similar, so the relative acid amount of catalysts were normalized by the peak area of the desorbed peak and shown in Table 3. Noticeably, the amount of acid of Ni_xMn-LDO catalysts at the weak acid sites decreased and increased at strong acid sites gradually with the increase of Ni/Mn molar ratios, which suggest that the acid sites on the surface of catalyst are related to the relative distribution of Ni and Mn elements. In addition, Ni_5Mn-LDO catalyst displayed more amount of acid than others, which implied that more NH_3 can be adsorbed on the catalyst surface and further promote the low-temperature NH_3-SCR reaction. What's more, the acid

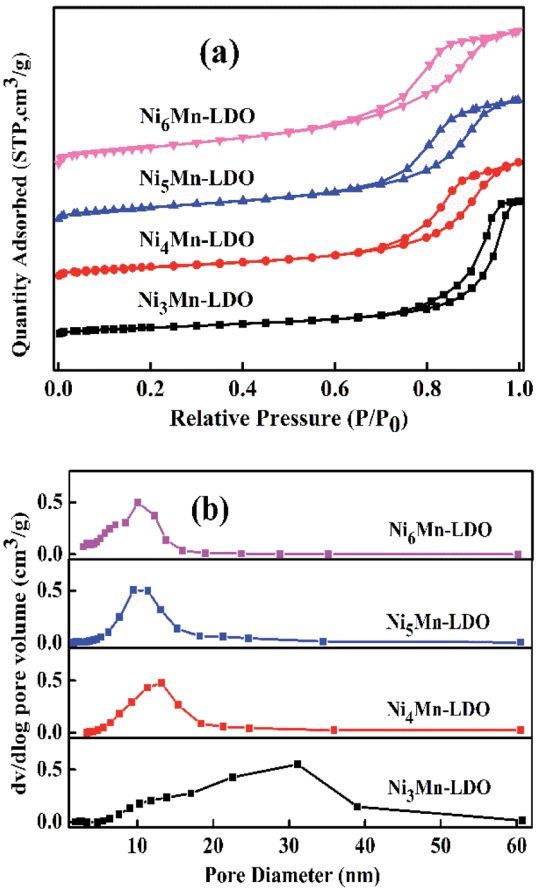

Fig. 8 (a) N_2 adsorption–desorption isotherms and (b) pore diameter distribution of Ni_xMn-LDO (x = 3, 4, 5, 6) catalysts.

Table 2 The information of surface area and pore structure distribution of Ni_xMn-LDO (x = 3, 4, 5, 6) catalysts

Samples	S_{BET} ($m^2\ g^{-1}$)	D_{BJH} (nm)	V_{total} ($cm^3\ g^{-1}$)
Ni_3Mn-LDO	41	17.71	0.23
Ni_4Mn-LDO	53	11.19	0.15
Ni_5Mn-LDO	70	9.35	0.17
Ni_6Mn-LDO	83	7.73	0.19

amount distribution of the four catalysts has a similar order to the size of the metal oxide particles. This results suggest that the uniform distribution of the active species particles is an crucial factor on the full exposure of the acid sites on the catalyst surface.

3.2.6 H_2-TPR analysis. The redox capability of the catalysts is another indispensable indicator for evaluating catalytic activity in the NH_3-SCR reaction. The H_2-TPR results of four catalysts was demonstrated in Fig. 10. There are two reduction peaks on the curves, the first peak appears in the temperature range of 350–395 °C, corresponding to the process: $Ni_6MnO_8 + H_2 \rightarrow MnO–NiO + H_2O$, which represents the reduction from MnO_x species to MnO; the second step of the reduction takes place at 405–446 °C and can be attributed to: $MnO–NiO + H_2$

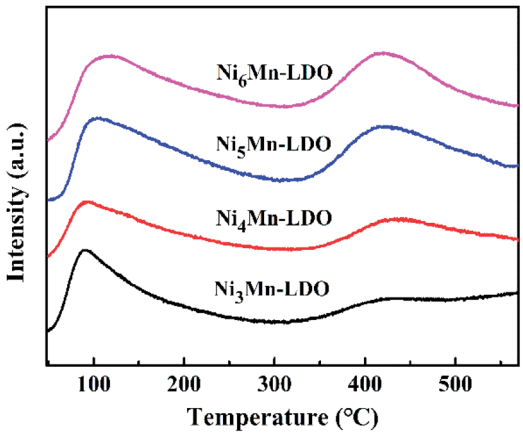

Fig. 9 NH_3-TPD curves of Ni_xMn-LDO (x = 3, 4, 5, 6) catalysts.

Table 3 Relative amount and proportion of NH_3 desorption for Ni_xMn-LDO (x = 3, 4, 5, 6) catalysts

Samples	Total amount of NH_3 desorption	Proportion of NH_3 desorption (%)	
		Weak acid site (50–300 °C)	Strong acid site (350–550 °C)
Ni_3Mn-LDO	1.00	88.4	11.6
Ni_4Mn-LDO	1.08	67.4	32.6
Ni_5Mn-LDO	2.10	62.2	37.8
Ni_6Mn-LDO	1.91	59.6	40.4

$\rightarrow Ni + MnO + H_2O$, indicating the transformation of NiO species to Ni.[20,39,53,54] Likewise, it can be observed that the positions of the reduction peaks of four catalysts have changed significantly. Obviously, with the increase of Ni/Mn molar ratios, the peak position of Ni_xMn-LDO catalysts shifted to the lower temperature, which suggests that the reduction process is becoming easier. Especially, Ni_5Mn-LDO catalyst shows the lowest reduction peak temperature and correspondingly the highest catalytic activity. The reason may be related to the uniform dispersion of the reducible species on the surface of

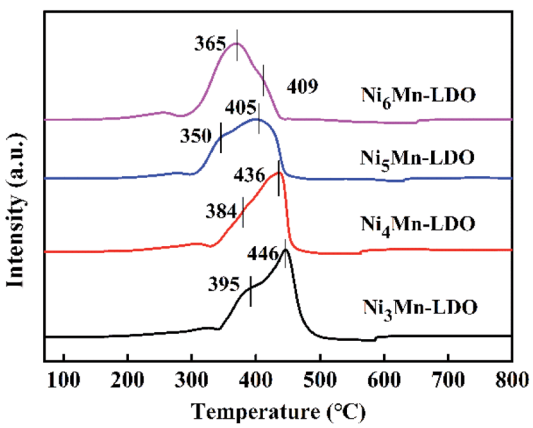

Fig. 10 H_2-TPR curves of Ni_xMn-LDO (x = 3, 4, 5, 6) catalysts.

catalyst, which can be confirmed by BET and TEM analysis results.

3.2.7 SO_2 & H_2O resistance and stability tests. In actual NH_3-SCR reaction conditions, the flue gas inevitably contains trace amount of SO_2 and H_2O, which can greatly affect the $DeNO_x$ performance of catalyst at low temperature.[55] So, it is necessary to study the SO_2 & H_2O resistance of catalyst. Fig. 11(a) illustrates SO_2 & H_2O resistance tests of Ni_5Mn-LDO catalyst at 240 °C under a GHSV of 45 000 h^{-1}. When SO_2 was introduced into the mixture gases, NO_x conversion of catalyst started to decrease from the original 98% and gradually tended to a smooth value of 88%. And then adding 10 vol% H_2O into reaction system, where SO_2 and H_2O coexisted, $DeNO_x$ performance of this catalyst was further suppressed. Upon removing SO_2, NO_x conversion has risen and remained at around 86%. After further closing H_2O, NO_x conversion can be restored to 92%, but still slightly lower than the initial value, which may be due to the deposition of ammonium sulfate on the surface of the catalyst. In general, Ni_5Mn-LDO catalyst presented considerable SO_2 & H_2O resistance.

It is also an important challenge for the catalysts to maintain high $DeNO_x$ efficiency for a long time in the NH_3-SCR reaction. The stability test of Ni_5Mn-LDO catalyst was depicted in Fig. 11(b). As can be seen, NO_x conversion has only a slight decrease with the extension of the test time throughout the test range, which suggest that the catalyst has good stability.

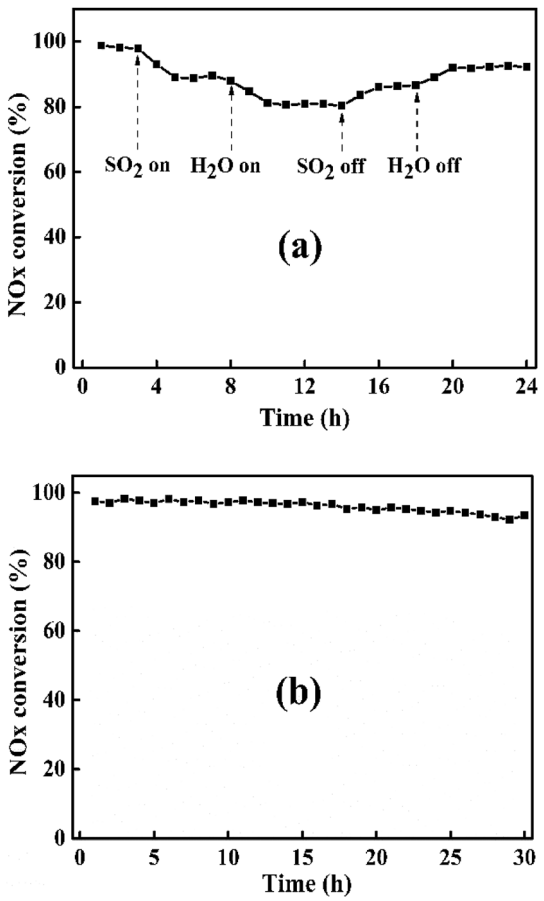

Fig. 11 (a) SO_2 & H_2O resistance test and (b) stability test of Ni_5Mn-LDO catalyst at 240 °C. Reaction conditions: [NO] = [NH_3] = 600 ppm, [O_2] = 5 vol%, SO_2 = 100 ppm (when used), 10 vol% H_2O (when used), N_2 as balance gas, GHSV = 45 000 h^{-1}.

4. Conclusions

A series of Ni_xMn-LDO ($x = 3, 4, 5, 6$) metal oxides were obtained by calcining Ni_xMn-LDHs ($x = 3, 4, 5, 6$) precursors at 400 °C and were employed as NH_3-SCR catalysts. The catalytic results presented that all catalysts exhibited good SCR activity and N_2 selectivity, which might be attributed to the formation of Ni_6MnO_8 active species. In addition, catalytic performance of Ni_xMn-LDO catalysts were sensitive to the Ni/Mn molar ratios, which were related to the redox capacity and surface acidity caused by dispersion. In fact, it was demonstrated that the distribution of active species particles on the surface of catalyst could be improved by optimizing the morphology of the Ni_xMn-LDHs precursors. This study provides a new method to prepare catalyst with good dispersion properties by calcining LDHs precursors.

Conflicts of interest

There are no conflicts of interest to declare.

Acknowledgements

The project was supported by National Natural Science Foundation of the China (No. 21073131), Natural Science Foundation of Shanxi Province, China (No. 201601D102007).

Notes and references

1 K. Liu, H. He, Y. B. Yu, Z. D. Yan, W. W. Yang and W. P. Shan, *J. Catal.*, 2019, **369**, 372–381.
2 D. Damma, P. R. Ettireddy, B. M. Reddy and P. G. Smirniotis, *Catalysts*, 2019, **9**, 349.
3 P. Forzatti, I. Nova and E. Tronconi, *Angew. Chem., Int. Ed.*, 2009, **121**, 8516–8518.
4 Z. B. Zhi, X. Ning, F. Zhou, B. Yang, Y. W. Tu, J. Jin, W. Lu and Z. H. Liu, *RSC Adv.*, 2018, **8**, 21915–21925.
5 Z. H. Chen, Q. Yang, H. Li, X. H. Li, L. F. Wang and S. C. Tsang, *J. Catal.*, 2010, **276**, 56–65.
6 R. H. Gao, D. S. Zhang, X. G. Liu, L. Y. Shi, P. Maitarad, H. R. Li, J. P. Zhang and W. G. Cao, *Catal. Sci. Technol.*, 2013, **3**, 191–199.
7 F. Kapteijn, L. Singoredjo, A. Andreini and J. A. Moulijn, *Appl. Catal., B*, 1994, **3**, 173–189.
8 X. L. Tang, J. M. Hao, W. G. Xu and J. H. Li, *Catal. Commun.*, 2007, **8**, 329–334.
9 X. F. Tang, J. H. Li, L. Sun and J. M. Hao, *Appl. Catal., B*, 2010, **99**, 156–162.
10 J. H. Li, H. Z. Chang, L. Ma, J. M. Hao and R. T. Yang, *Catal. Today*, 2011, **175**, 147–156.
11 C. Liu, J. W. Shi, C. Gao and C. M. Niu, *Appl. Catal., A*, 2016, **522**, 54–69.

12 M. Casapu, O. Kröcher and M. Elsener, *Appl. Catal., B*, 2009, **88**, 413–419.
13 M. Kang, E. D. Park, J. M. Kim and J. E. Yie, *Catal. Today*, 2006, **111**, 236–241.
14 Z. H. Chen, X. H. Li, X. Gao, Y. B. Jiang, Y. X. Lü, F. R. Wang and L. F. Wang, *J. Catal.*, 2009, **30**, 4–6.
15 Z. H. Lian, F. D. Liu, H. He, X. Y. Shi, J. S. Mo and Z. B. Wu, *Chem. Eng. J.*, 2014, **250**, 390–398.
16 Y. Wan, W. R. Zhao, Y. Tang, L. Li, H. J. Wang, Y. L. Cui, J. L. Gu, Y. S. Li and J. L. Shi, *Appl. Catal., B*, 2014, **148**, 114–122.
17 L. Q. Chen, X. Y. Niu, Z. B. Li, Y. L. Dong, Z. P. Zhang, F. L. Yuan and Y. J. Zhu, *Catal. Commun.*, 2016, **85**, 48–51.
18 H. R. Li, D. S. Zhang, P. P. Maitarad, L. Y. Shi, R. H. Gao, J. P. Zhang and W. G. Cao, *Chem. Commun.*, 2012, **48**, 10645–10647.
19 Y. L. Han, J. C. Mu, X. Y. Li, J. S. Gao, S. Y. Fan, F. Tan and Q. D. Zhao, *Chem. Commun.*, 2018, **54**, 9797–9800.
20 S. X. Cai, D. S. Zhang, L. Y. Shi, J. Xu, L. Zhang, L. Huang, H. R. Li and J. P. Zhang, *Nanoscale*, 2014, **6**, 7346.
21 J. Xiong, Q. Q. Wu, X. L. Mei, J. Liu, Y. C. Wei, Z. Zhao, D. Wu and J. M. Li, *ACS Catal.*, 2018, **8**, 7915–7930.
22 Y. F. Zhao, S. He, M. Wei, D. G. Evans and X. Duan, *Chem. Commun.*, 2010, **46**, 3031–3033.
23 H. Yan, M. Wei, J. Ma, F. Li, D. G. Evans and X. Duan, *J. Phys. Chem. A*, 2009, **113**, 6133–6141.
24 Q. Wang and D. O'Hare, *Chem. Rev.*, 2012, **112**, 4124–4155.
25 X. Wu, R. N. Wang, Y. L. Du, C. L. Zhou, H. Meng and X. M. Xie, *Mol. Catal.*, 2019, **467**, 150–160.
26 W. Y. Zhou, Q. Y. Tao, F. Sun, X. B. Cao, J. F. Qian, J. Xu, M. Y. He, Q. Chen and J. L. Xiao, *J. Catal.*, 2018, **361**, 1–11.
27 J. W. Zhao, J. L. Chen, S. M. Xu, M. F. Shao, Q. Zhang, F. Wei, J. Ma, M. Wei, D. G. Evans and X. Duan, *Adv. Funct. Mater.*, 2014, **24**, 2938–2946.
28 X. J. Li, M. Y. Xin, S. Guo, T. H. Cai, D. F. Du, W. Xing, L. M. Zhao, W. Y. Guo, Q. Z. Xue and Z. F. Yan, *Electrochim. Acta*, 2017, **253**, 302–310.
29 W. Ma, R. Z. Ma, J. H. Wu, P. Z. Sun, X. H. Liu, K. C. Zhou and T. Sasaki, *Nanoscale*, 2016, **8**, 10425–10432.
30 S. Miyata, *Clays Clay Miner.*, 1975, **23**, 369–375.
31 Q. H. Yan, S. N. Chen, L. Qiu, Y. S. Gao, D. O'Hare and Q. Wang, *Dalton Trans.*, 2017, **47**, 2992–3004.
32 R. N. Wang, X. Wu, C. L. Zhou, X. J. Li and Y. L. Du, *Catalysts*, 2018, **8**, 384.
33 Q. H. Yan, S. N. Chen, C. Zhang, D. O'Hare and Q. Wang, *J. Colloid Interface Sci.*, 2018, **526**, 63–74.
34 S. P. Mo, S. D. Li, W. H. Li, J. Q. Li, J. Y. Chen and Y. F. Chen, *J. Mater. Chem. A*, 2016, **4**, 8113–8122.
35 Z. P. Xu, L. Li, C. Y. Cheng, R. G. Ding and C. H. Zhou, *Appl. Clay Sci.*, 2013, **74**, 102–108.
36 X. Xiang, H. I. Hima, H. Wang and F. Li, *Chem. Mater.*, 2007, **20**, 1173–1182.
37 X. Wu, Y. L. Feng, Y. L. Du, X. Z. Liu, C. L. Zou and Z. Li, *Appl. Surf. Sci.*, 2019, **467**, 802–810.
38 J. J. Zhang, R. R. Hu, P. Dai, Z. M. Bai, X. X. Yu, M. Z. Wu and G. Li, *J. Mater. Sci.: Mater. Electron.*, 2018, **29**, 7510–7518.
39 Y. G. Zhang, Z. F. Qin, G. F. Wang, H. Q. Zhu, M. Dong, S. N. Li, Z. W. Wu, Z. K. Li, Z. H. Wu, J. Zhang, T. D. Hu, W. B. Fan and J. G. Wang, *Appl. Catal., B*, 2013, **129**, 172–181.
40 H. Meng, J. N. Liu, Y. L. Du, B. H. Hou, X. Wu and X. M. Xie, *Appl. Catal., A*, 2019, **119**, 101–105.
41 L. Zhang, L. Y. Shi, L. Huang, J. P. Zhang, R. H. Gao and D. S. Zhang, *ACS Catal.*, 2014, **4**, 1753–1763.
42 Q. Liu, J. J. Gao, F. N. Gu, X. P. Lu, Y. J. Liu, H. F. Li, Z. Y. Zhong, B. Liu, G. W. Xu and F. B. Su, *J. Catal.*, 2015, **326**, 127–138.
43 X. Wu, X. J. Li, Y. L. Du, R. N. Wang, X. M. Guo and B. H. Hou, *ChemCatChem*, 2019, **11**, 1993–2003.
44 S. Ali, L. Q. Chen, Z. B. Li, T. R. Zhang, R. Li, S. U. H. Bakhtiar, X. S. Leng, F. L. Yuan, X. Y. Niu and Y. J. Zhu, *Appl. Catal., B*, 2018, **236**, 25–35.
45 Y. Li, G. Q. Li, Y. Lu, W. X. Hao, Z. Wei, J. Liu and Y. F. Zhang, *Mol. Catal.*, 2018, **445**, 21–28.
46 L. Lietti, I. Nova, G. Ramis, L. D. Acqua, G. Busca, E. Giamello, P. Forzatti and F. Bregani, *J. Catal.*, 1999, **187**, 419–435.
47 Z. B. Wu, B. Q. Jiang, Y. Liu, H. Q. Wang and R. B. Jin, *Environ. Sci. Technol.*, 2007, **41**, 5812–5817.
48 C. Fang, D. S. Zhang, L. Y. Shi, R. H. Gao, H. R. Li, L. P. Ye and J. P. Zhang, *Catal. Sci. Technol.*, 2013, **3**, 803–811.
49 S. Roy, B. Viswanath, M. S. Hegde and G. Madras, *J. Phys. Chem. C*, 2008, **112**, 6002–6012.
50 Y. Peng, W. W. Yu, W. K. Su, X. Huang and J. H. Li, *Catal. Today*, 2015, **242**, 300–307.
51 M. Mhamdi, S. Khaddar-Zine and A. Ghorbel, *Appl. Catal., A*, 2009, **357**, 42–50.
52 L. Zhang, D. S. Zhang, J. P. Zhang, S. X. Cai, C. Fang, L. Huang, H. R. Li, R. H. Gao and L. Y. Shi, *Nanoscale*, 2013, **5**, 9821–9829.
53 L. Christel, A. Pierre and D. A.-M. R. Abel, *Thermochim. Acta*, 1997, **306**, 51–59.
54 C. Laberty, J. Pielaszek, P. Alphonse and A. Rousset, *Solid State Ionics*, 1998, **110**, 293–302.
55 K. Skalska, J. S. Miller and S. Ledakowicz, *Sci. Total Environ.*, 2010, **408**, 3976–3989.